Horizontal wavenumber spectra of MLS radiance fluctuations

Dong L. Wu *

Jet Propulsion Laboratory, California Institute of Technology, Pasadena, 4800 Oak Grove Dr., Pasadena, CA 91109, USA

Abstract

Radiance fluctuations from Upper Atmosphere Research Satellite Microwave Limb Sounder (UARS MLS) reflect atmospheric temperature oscillations of short ($\geqslant 30\,\text{km}$) horizontal and long ($>10\,\text{km}$) vertical wavelengths at 38–80 km altitudes. These radiance fluctuations often show wave-like structures with clear phase coherence among different altitudes. This paper applies a spectral analysis to MLS limb-tracking radiances and obtains a seasonal climatology of horizontal wavenumber spectra at scales of 50–800 km for 6 altitudes (38, 43, 48, 53, 61 and 80 km) and 8 latitudes (from 70°S to 70°N). Most of the power spectra exhibit a slope close to -2 but some can be as steep as -3 in wave active regions. The spectral power density is strongly season-and-latitude dependent in the stratosphere, which is thought largely due to the modulation of the background winds on the vertical wavenumber spectrum. The spectral amplitudes grow exponentially with height between 38 and 50 km but the growth rate becomes small or close to zero near and above 50 km. The growth rates at 38–53 km altitudes are scale-dependent showing less efficient vertical propagation for larger-scale waves. The near-zero growth in the lower mesosphere is thought mainly due to wave saturation/breaking at these altitudes. © 2001 Elsevier Science Ltd. All rights reserved.

Keywords: Gravity wave spectrum; Temperature fluctuations; Satellite observations

1. Introduction

Gravity wave spectra contain important information about wave generation, propagation, breakdown, and interaction with the background atmosphere. At small vertical or temporal scales, observations often show a nearly universal spectral shape, which is characterized by a slope of $-5/3$ in frequency spectra and -3 in vertical wavenumber spectra (Gage, 1979; Balsley and Carter, 1982; Van Zandt, 1982). These findings have greatly stimulated gravity-wave research in recent years. The universality in the wave spectra is thought due to the so-called wave saturation/breaking that prevents wave amplitudes from further growing with height (e.g. Fritts, 1984). However, the physical mechanisms behind the wave saturation are yet to be agreed upon. The theories proposed include shear and convective instabilities (Dewan and Good, 1986; Smith et al., 1987),

dissipation from nonlinear interactions (Weinstock, 1990) and Doppler-spreading due to advective nonlinearity (Hines, 1991, among others). Despite the unsolved puzzle about formation of the universal spectra, gravity wave breaking has been well recognized as one of the most important forcings that drive global circulations in the middle atmosphere (Lindzen, 1981; Matsuno, 1982; Holton, 1982). For a more quantitative understanding of atmospheric dynamics, global distributions and characteristics of breaking gravity waves are needed.

Most observations of gravity wave spectra are provided by ground-based radar/lidar techniques which have good temporal and vertical resolutions (Manson and Meek, 1986; Vincent and Fritts, 1987; Wilson et al., 1991; Fukao et al., 1994). A better vertical resolution has been obtained with balloon/rocket in situ measurements which can detect small-scale fluctuations in the troposphere and stratosphere (Allen and Vincent, 1995; Hirota, 1984; Eckermann et al., 1994; Wu and Widdel, 1991). To measure horizontal structures of gravity waves, aircraft, space

* Tel.: +1-818-393-1954; fax: +1-818-393-5065.
E-mail address: dwu@mls.jpl.nasa.gov (D.L. Wu).

shuttle and airglow techniques were used but limited in time, latitude and height coverage (Nastrom and Gage, 1985; Fritts et al., 1989; Swenson et al., 1995; Bacmeister et al., 1996). Using satellite remote sensing techniques to measure gravity-wave-induced fluctuations is difficult but feasible. Fetzer and Gille (1994) attempted to derive vertical wavenumber spectra from Limb Infrared Monitor of the Stratosphere (LIMS) temperature measurements but their results were somewhat on larger scales than that observed with ground-based techniques. Compared to frequency and vertical wavenumber observations, experimental studies on the horizontal wave spectrum remain limited.

Recently, Wu and Waters (1996b) (hereafter WW96b) obtained small-scale (∼100 km) temperature variances from the saturated radiances measured by the Upper Atmosphere Research Satellite Microwave Limb Sounder (UARS MLS). The MLS 63 GHz radiometer provides ∼6 years of stable, low-noise, and regularly sampled radiance data that can be used for small-scale wave studies. The study by Wu and Waters (1997) (hereafter WW97) showed that MLS radiances are quite sensitive to temperature fluctuations induced by gravity waves of short (∼100 km) horizontal and long (> 10 km) vertical wavelengths. Several interesting features are uncovered in the radiance variance maps, including high correlation between enhanced variances and deep convection zones in the summer troposphere and strong winds in winter polar vortices. In the stratosphere the variance amplitude grows exponentially with height as expected for free propagating gravity waves while in the mesosphere the growth is nearly zero at high winter latitudes and in the summer subtropics. The strong geographical variation is mainly due to background wind modulations but the near-zero growth is thought as a consequence of wave saturation/breaking at these altitudes (WW96b). Effects of background winds on MLS radiance fluctuations are further explored with model simulations by Alexander (1998) who showed that the background wind modulation can explain most of the latitudinal and seasonal variations of MLS variances in the stratosphere.

Wu and Waters (1996a) further investigated MLS radiance fluctuations observed with a limb-tracking mode. In this observing geometry, MLS antenna keeps tracking a fixed tangent height, producing a continuous sampling of atmospheric temperature. Such a data set is particularly useful for gravity wave studies because of high horizontal resolution (∼15 km along the track) and long data sequence. The limb-tracking observation is not the normal operation mode and only available after 1994 with a limited number of days. Wu and Waters (1996a) showed that the limb-tracking data contain many interesting wave-like features with clear amplitude growth with height and phase coherence among the fluctuations at different altitudes.

To further explore the characteristics of MLS radiance fluctuations, this paper is aimed to study horizontal wavenumber spectra of the limb-tracking radiances and produce a seasonal climatology of such spectra as a function altitude and latitude. The paper is organized such that MLS radiance fluctuations and data analyzing methods are described in the next section, followed by the spectral results for December–February and March–May (Section 3). Interpretations and discussions are given in Section 4.

2. Data analysis

MLS viewing geometry, measurement precision, and orientation of temperature weighting function are essential for the instrument to sense weak gravity-wave-scale atmospheric fluctuations. One must understand the characteristics of these instrument variables before correctly interpreting variations associated with the radiance fluctuations. For the saturated limb radiances, the temperature weighting functions have a cigar-like shape that is orientated along the line-of-sight (LOS) direction (Fig. 1(a)). Because of this tilting nature, the observed amplitude of radiance fluctuations may depend upon the angle between the instrument viewing and wave propagating directions. This angle determines how gravity waves are averaged by the instrument weighting function and what amplitude is observed in the radiance fluctuations. For the same wave the amplitude of radiance fluctuations may differ significantly between ascending and descending orbits due to the viewing angle differences. Roughly speaking, MLS weighting function is a volume of ∼150 km along LOS, ∼20 km across LOS and ∼10 km in the vertical direction. It is difficult for MLS to detect waves of vertical wavelengths less than 10 km due to the weighting function averaging in the vertical direction. Similarly, it is hard for the instrument to detect waves of horizontal wavelengths shorter than 150 km along LOS. However, MLS has a better horizontal resolution in the cross-LOS or along-track direction. This horizontal resolution is ∼30 km, which is limited mainly by the antenna beamwidth (∼20 km) and MLS integration time (∼15 km) (Fig. 1(b)). Prolonged MLS footprints imply that the instrument is selective about wave propagation direction. Generally speaking, MLS is more sensitive to waves that propagate meridionally than zonally at most latitudes.

In this study we use all the limb-tracking radiances available during 1994–1997. Fig. 2 gives some examples showing the saturated radiances during limb tracking at the ∼18 km tangent height. The height where the radiance is saturated depends primarily upon absorption coefficients or frequency differences from the O_2 line center but a little upon viewing condition. For frequency closer to the line center, stronger atmospheric absorption is expected, and therefore the limb radiance is saturated at a higher altitude. There are 15 spectral channels in the 63 GHz radiometer distributed symmetrically about the O_2 line, measuring 8 different altitude layers from 28 to 80 km. We only use channels 3–8 on one side of the O_2 line, which gives six

(a)

(b)
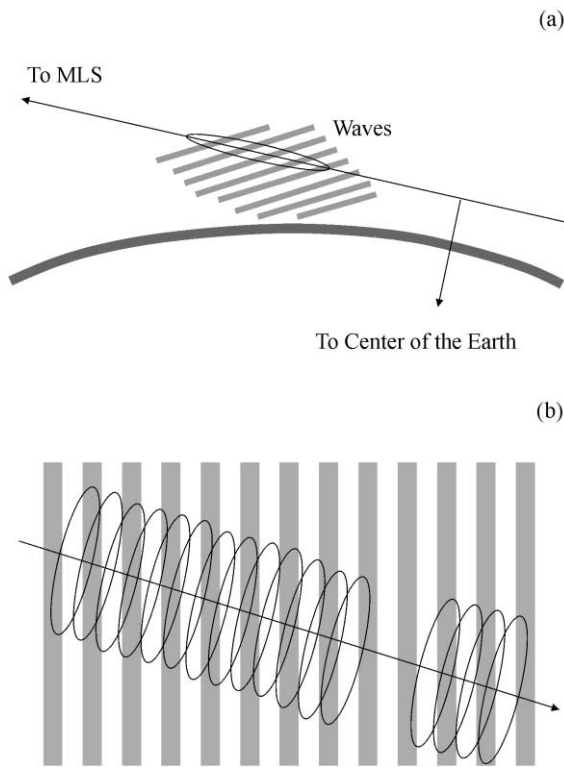
Fig. 1. Schematic diagrams to illustrate MLS viewing geometry and weighting function. (a) MLS weighting function of saturated radiances has a cigar-like shape on the near side of the tangent point. The weighting function performs a volume average over small-scale atmospheric temperature fluctuations such that the resulting amplitude of radiance perturbations is much smaller than the actual temperature fluctuations. (b) In the horizontal plane MLS footprints are asymmetric, making them very selective to wave propagating directions. Since MLS views 90° from the flight direction and UARS orbit has 57° inclination, the meridionally propagating waves become more sensitive.

altitudes at 38, 43, 48, 53, 61 and 80 km. As discussed in WW96b, the radiance fluctuations are contributed mostly by atmospheric temperature oscillations and instrument noise. The instrument noise can be treated as a stationary white source, not varying with measurement location and time. Therefore, the geographical and seasonal variations in the radiance variance/power spectra are basically due to atmospheric variability.

Two examples in Fig. 2 are the MLS radiance measurements over a half-orbit, illustrating some interesting features in the radiance fluctuations. Fig. 2(a) exhibits a sharp disturbance of ~200 km near 55°N that was observed from orbit 12 on 4 March 1995. The amplitude of this wave-like oscillation grows with height from ~1K at ~38 km (channel 3) to ~5K at ~53 km (channel 6) and shows little phase tilting with height. Other oscillations are also evident in this re-

gion, which have somewhat larger (300–500 km) scales and seem related to the sharp disturbance at 55°N. The phase of these large-scale features is tilted with respect to height, leaning toward the pole. This event was either very transient or very localized since it did not repeat next day for the same orbit that was ~200 km away.

Fig. 2(b) shows another example of wave-like features that have a much larger scale (~1000 km), clear amplitude growth and phase shift with height. From channel 3 (~38 km) to channel 7 (~61 km) its phase moves poleward by ~600 km, which would correspond to a large phase speed in the meridional direction. Superimposed on the top of the large-scale wave are many smaller-scale waves, also growing with height in amplitude. By the time they reaches ~61 km the amplitude of small-scale waves is about a half of the larger-scale one, making the larger-scale wave less distinguishable.

During December 1994–September 1997, MLS made 178 days of limb-tracking observations, among which 61 days are for December–February (DJF), 54 days for March–May (MAM), 33 days for June–August (JJA), and 30 days for September–November (SON). On a given day, MLS observations cover latitudes from 34° in one hemisphere to 80° in the other depending whether it looks south or north of the orbit. UARS makes 10 yaw maneuvers each year allowing alternating views of high latitudes in the two hemispheres. Therefore, the numbers of south/north viewing days are important for the statistics at high latitudes, and they are 12/49, 32/22, 21/12, and 18/12, respectively, for DJF, MAM, JJA, and SON.

Fast Fourier transform (FFT) is employed to obtain radiance horizontal-wavenumber spectra. The data series are truncated to 134-point segments, corresponding to a distance of ~2010 km since the satellite travels ~15 km between two adjacent samples. The truncations are not overlapped and we are only interested in the horizontal wavelengths less than 1000 km. Because the individual spectrum is highly fluctuated, the spectra are averaged for each season and latitude bin in order to achieve statistically reliable results. With enough averaging, one can assess the noise power to good accuracy so as to extract weak atmospheric spectral power near or below the noise level. The spectra are averaged into 8 latitudinal and 4 seasonal bins for climatological studies. Small data gaps, for example, due to calibration, are filled with linear interpolation while the series with a large gap (more than 34 points missing) are dropped. All truncated sequences are subject to a detrending process that removes mean and linear trend to reduce impacts of mean temperature and larger-scale waves. Following the detrending, the data are treated with the so-called pre-whitening process to further minimize influence of large-scale waves, and the post-darkening process to recover the actual spectral power density (e.g. Blackman and Tukey, 1958).

The final step in the spectral analysis is to subtract the instrument noise from the seasonally and zonally averaged radiance spectra by assuming a white distribution of the
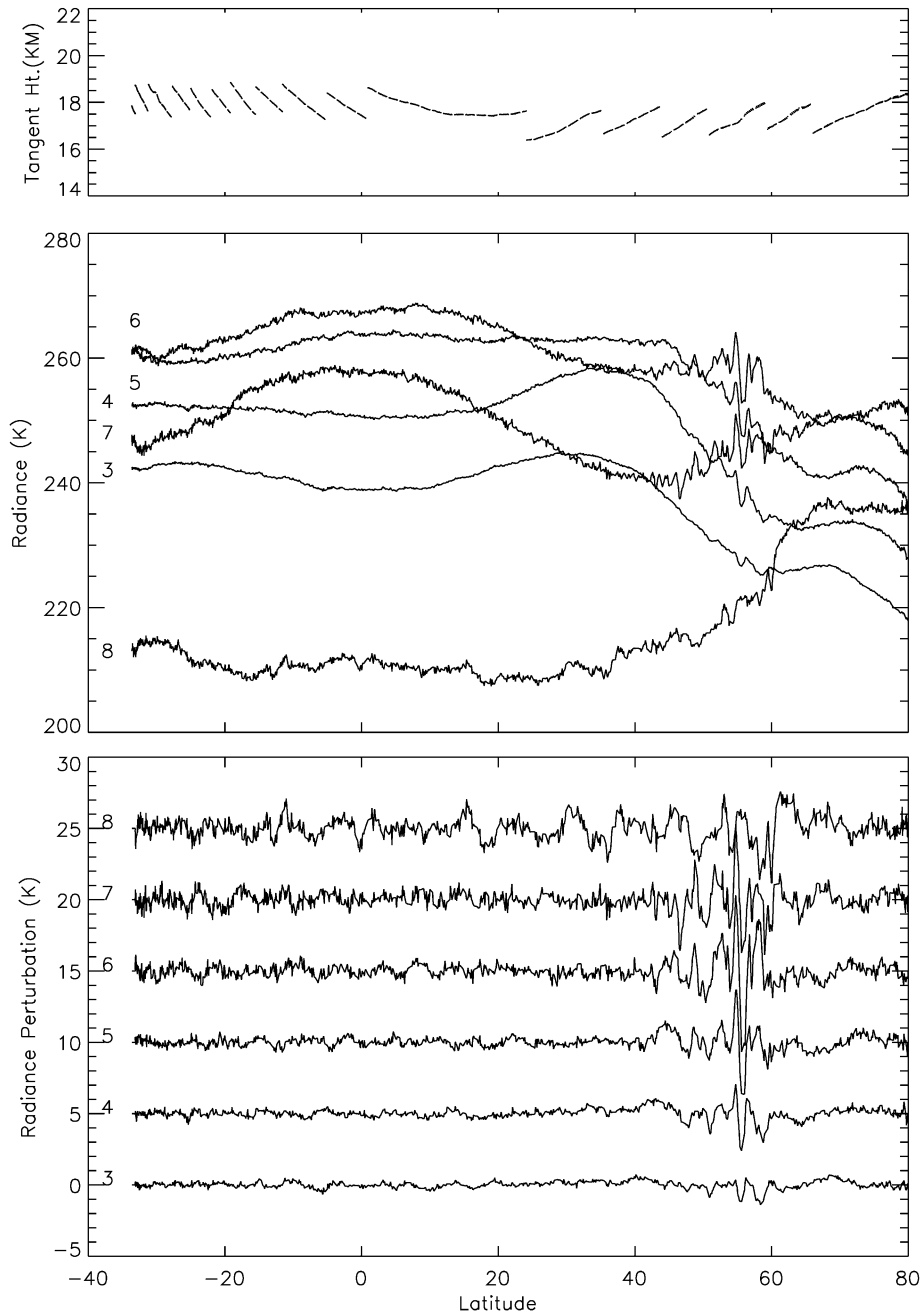
Fig. 2. Time series of MLS limb-tracking altitude (top), saturated radiances (middle) and radiance perturbations with large (> 1000 km) scale waves removed (bottom). The spectral channels of MLS radiances are labeled on the left of the time series. Radiance perturbations of different channels are offset by a 5K increment from channel 3. Two ascending orbits, (a) #12 and (b) #4 on 4 March 1995, are selected to show wave-like oscillations at several altitudes. Typical wave amplitude and phase variations are illustrated by these examples, showing phase lines both tilted and fixed with respect to height/channel. In these cases, waves of horizontal wavelengths between 200 and 500 km can be readily identified while waves of shorter scales are somewhat unclear due to smaller amplitudes and instrument noise.

noise spectrum. This correction extends the radiance spectrum to shorter wavelengths where the amplitudes are often near and below the noise level. MLS calibration data show that the instrument noise is a good white source and only channel-dependent. In practice, one can estimate the noise power from the radiance spectra at scales smaller than 40 km.
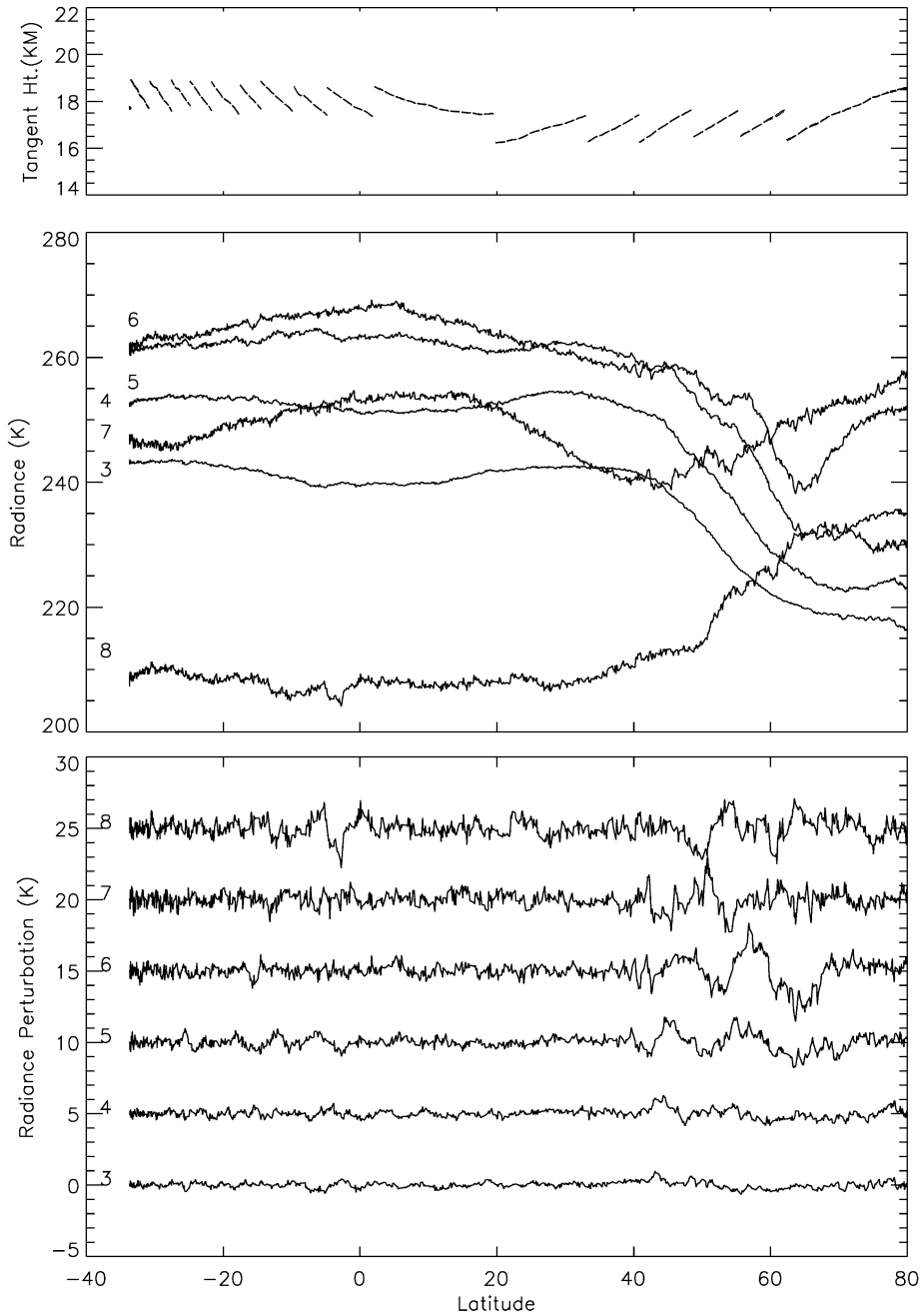
Fig. 2. (*continued*)

3. Results

For each seasonal climatology there are a total of 48 spectra for 6 altitude (at 38, 43, 48, 53, 61, and 80 km) and 8 latitude bins (from 70°S to 70°N). In Fig. 3 are the 48 spectra for DJF, where (a) and (b) are the same spectra but grouped differently. Fig. 3(a) shows the spectra grouped by latitude to highlight wave amplitude growth with height and geographical variations. Fig. 3(b) shows the spectra grouped by altitude/channel to highlight variations due to geographical differences such as the background winds. Similarly, Figs. 4(a) and (b) are the spectra for MAM. JJA and SON results are not shown here since they are similar to those of DJF and MAM if one flips the two hemispheres. The estimated

noise powers are indicated by the horizontal lines in Figs. 3(a) and 4(a).

There are significant hemispheric differences of the wave spectra during DJF (Fig. 3(a)). The spectra in the Northern Hemisphere (NH) generally have larger amplitudes and steeper slopes in the stratosphere than those in the Southern Hemisphere (SH). The spectral slope of 50–500 km scales varies from −2 to −3 in wave active regions, showing large differences of spectral power density at long wavelengths. On the other hand, the hemispheric difference reduces at higher altitudes as wave amplitudes become larger, but the general spectral characteristics remain to be the same. The

steeper slopes associated with larger amplitude spectra are still evident. Caution should be given to the spectra of small amplitudes, especially at wavelengths less than 50 km where wave amplitudes are far below the noise level, because they are sensitive to uncertainties of the noise estimated. For example, channel 3 spectra show oscillations or spikes at small scales that are likely due to a higher percentage of unsaturated radiances. This artificial effect could become worse for channel 1–2 radiances because the percentage of unsaturated radiances are higher for these wing channels. For conservative consideration, channel 1–2 radiances are excluded in this study. In addition, the feature showing a dip at ∼60 km
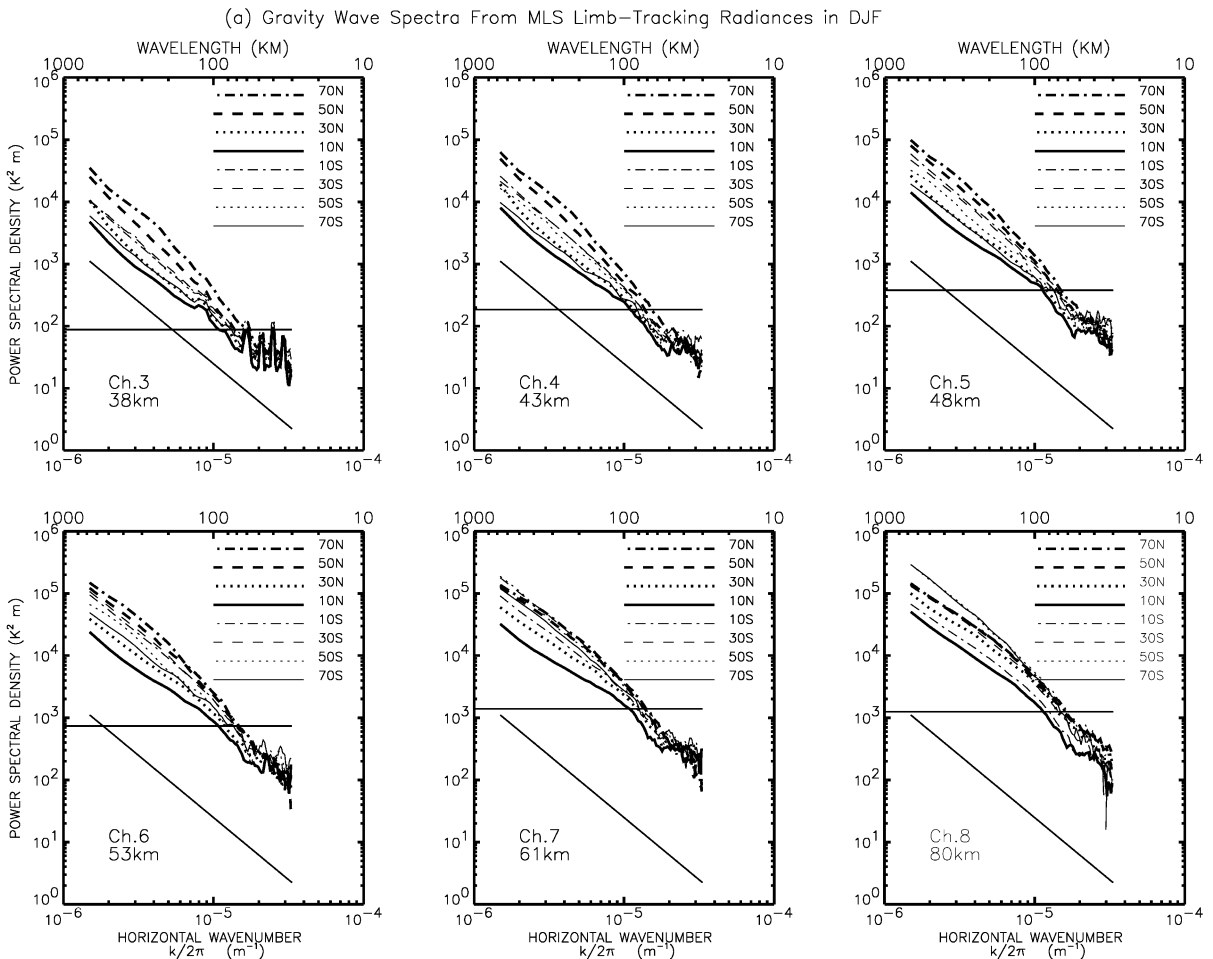
Fig. 3. Horizontal wavenumber spectra of MLS limb-tracking radiances for December–February. (a) MLS radiance spectra grouped by altitude (channel). A slope of −2 is shown as the reference and the horizontal line is the estimated noise level (see text). For channels 3–6 (or 38–53 km altitudes), the spectra have the largest magnitudes at 70°N while the weakest are at 10°N. For channels 7–8 (or 61–80 km altitudes), the spectral amplitudes at 70°N become comparable with those at 10–50°S due to the rapid growth in the southern hemisphere. Hemispheric differences are scale-dependent, showing larger amplitude separation at longer wavelengths. (b) The same spectra but grouped by latitude. Amplitude growth of these spectra is better shown this figure. The rate of growth with height, in terms of scale height, is calculated from channels 3–6 and shown by the thin line with its axis labeled on the right. The growth with a scale height of ∼7 km is expected for the free wave propagation in the atmosphere, and the larger the scale height, the more the loss. Larger-scale heights are generally seen at longer wavelengths suggesting that large-scale waves suffer more loss under the same atmospheric conditions.

(b) Gravity Wave Spectra From MLS Limb–Tracking Radiances in DJF
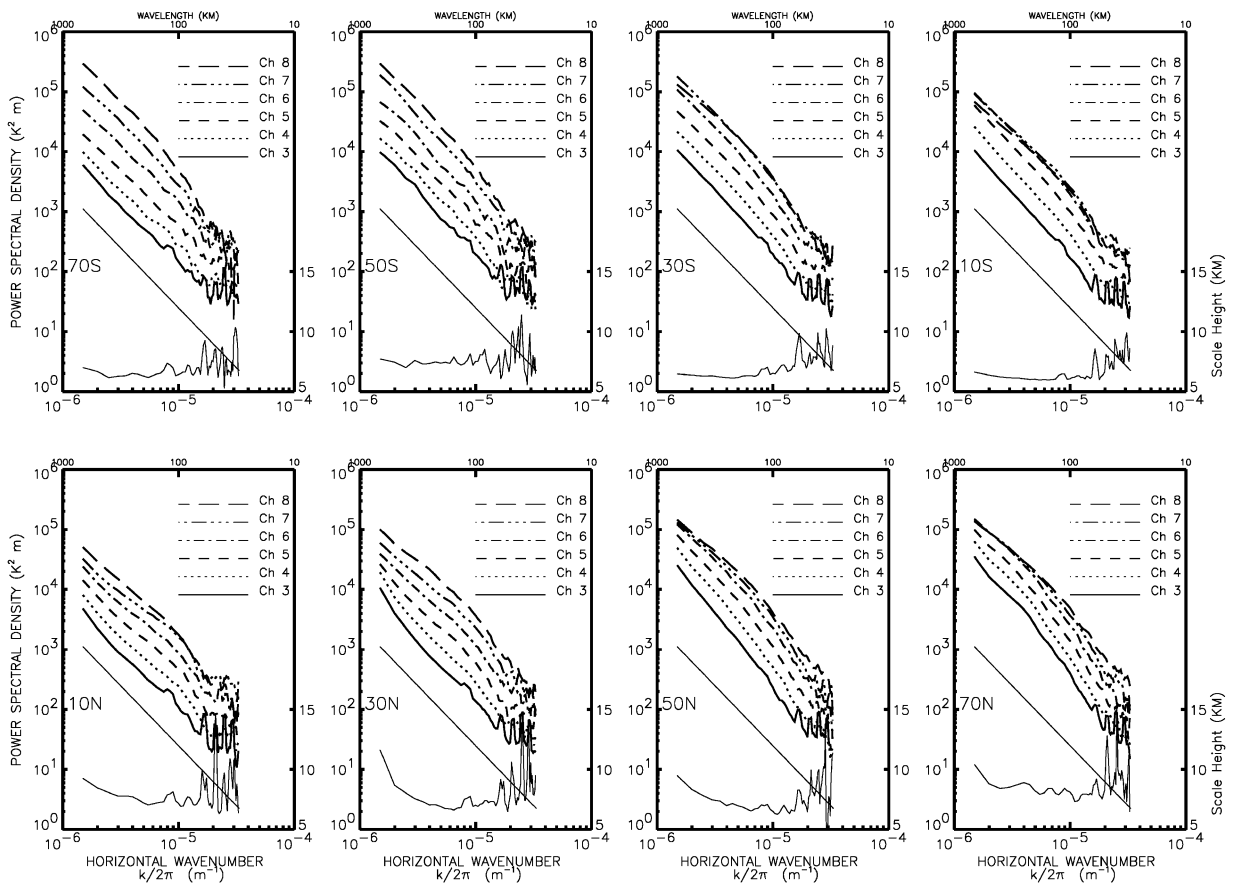
Fig. 3. (*continued*)

wavelength looks artificial as well because it appears in all the spectra analyzed. This artifact is likely due to missing data related to the routine calibration and will be discussed further later in the paper.

In Figs. 3(b) and 4(b) we use a scale height to characterize the rate of amplitude growth with height in the stratosphere, which is calculated from channel 3–6 spectra and is a function of wave scales and latitude. As shown in Fig. 3(b), most scale heights fall between 6 and 8 km in the upper stratosphere, which is expected for nearly free propagation of gravity waves. However, in some cases the scale height becomes greater than 8 km. For example, at 70°N the scale heights are near 9 km. In NH, the scale height generally increases with wavelength in the stratosphere but the growth rate approaches zero at heights above 53 km (channels 6–8). The slowdown in growth rate becomes obvious as the spectra of channels 6 and 7 (or 53 and 61 km) are overlapped on the top of each other. The near-zero growth in the mesosphere is also evident in Fig. 3(b) at latitudes of 30°S, 10°S, and 50°N, consistent with the variance results in WW96b (Fig. 4 therein). It is interesting to note that the near-zero growth occurs at all horizontal scales between 50 and 800 km. Perhaps the phenomenon is more pronounced at scales greater than 500 km. In the high-latitude SH, the spectral amplitude growth is strong at all scales in the stratosphere, showing a scale height of ~7 km. Such a growth rate allows the SH waves growing from small to large amplitudes over just two scale heights, and by the time when they reach ~61 km their amplitudes are in the same magnitude as the waves in the NH.

Compared to DJF spectra, MAM spectra have less hemispheric differences and smaller amplitudes in general (Fig. 4(a)). However, the major spectral characteristics are retained, showing similar height-dependent and scale-dependent variations. The spectral slope is shallower (less than −2) at larger scales and steeper (greater than −2) at shorter scales (<200 km). Also evident is that the slope at large wavelengths varies gradually from −2 at 38 and 43 km to somewhat below −2 at 53, 61, and 80 km. The spectral separation is not as large as in DJF at all altitudes but is clearly scale-dependent. Again, larger differences are seen at longer wavelengths.

Fig. 4(b) shows that the growth rate in MAM is roughly constant ($\sim$7 km) at 70–30°S but becomes scale-dependent at 10°S–70°N. The scale-dependent scale heights suggest that large-scale waves do not propagate as efficiently as small-scale waves in NH during MAM season. This is similar to the feature seen at 10–50°N during DJF. Small-scale waves pose a moderate growth rate (7–8 km) in both hemispheres. In the mesosphere, the growth rate approaches to zero for most horizontal scales at 70°S–10°N, and 70°N latitudes.

4. Discussions

MLS radiance fluctuations provide new information on gravity wave spectra in the middle atmosphere. Interpreta-

tion of the spectral features observed requires a thorough understanding of gravity wave propagation/breaking in the middle atmosphere as well as influence of MLS weighting function filtering. The purposes of this discussion is (1) to provide our best understanding about the instrument weighting function (its effects/limitations), and (2) to determine what are the gravity wave contributions and how they are related to the radiance spectra observed. Among the issues related to gravity wave propagation/breaking/saturation, we ask ourselves the following questions: (1) Is the near-zero growth in the mesosphere due to gravity wave saturation or the effect of a wind-shifted vertical wavenumber spectrum? (2) Why the wave growth is scale- and height-dependent? (3) What determines/maintains the slope of -2 in the spectra observed? We hope that the new observations would help better to understand the physics related to these issues.
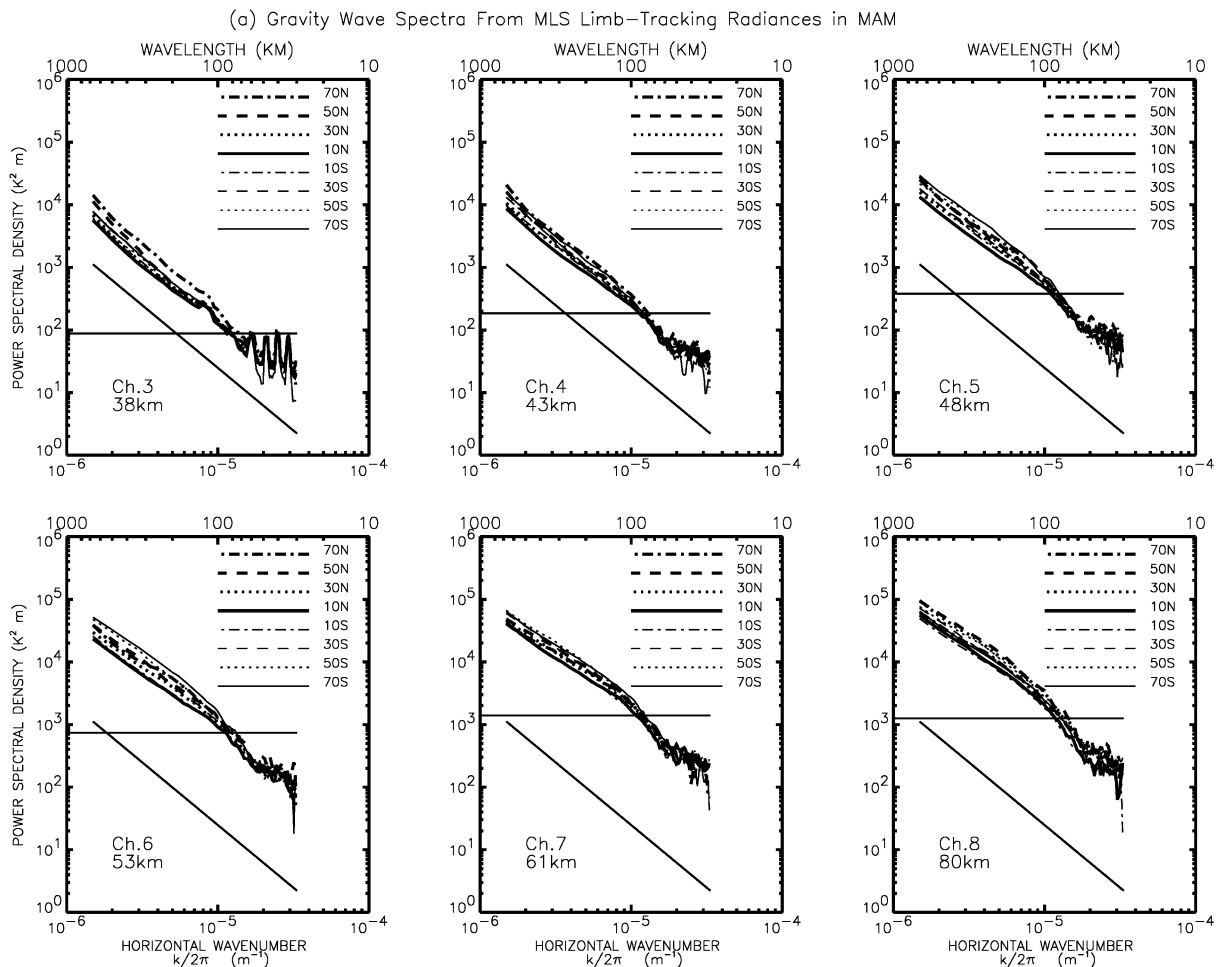
Fig. 4. Same as in Fig. 3 but for March–May. Spectra are less separated due to reduced strength of planetary wave activity in this season but the scale-dependent latitudinal differences are still evident. The scale-dependent amplitude growth is a common feature at all latitude bands. The scale heights at 10°S show the largest difference between long and short wavelengths.

(b) Gravity Wave Spectra From MLS Limb-Tracking Radiances in MAM
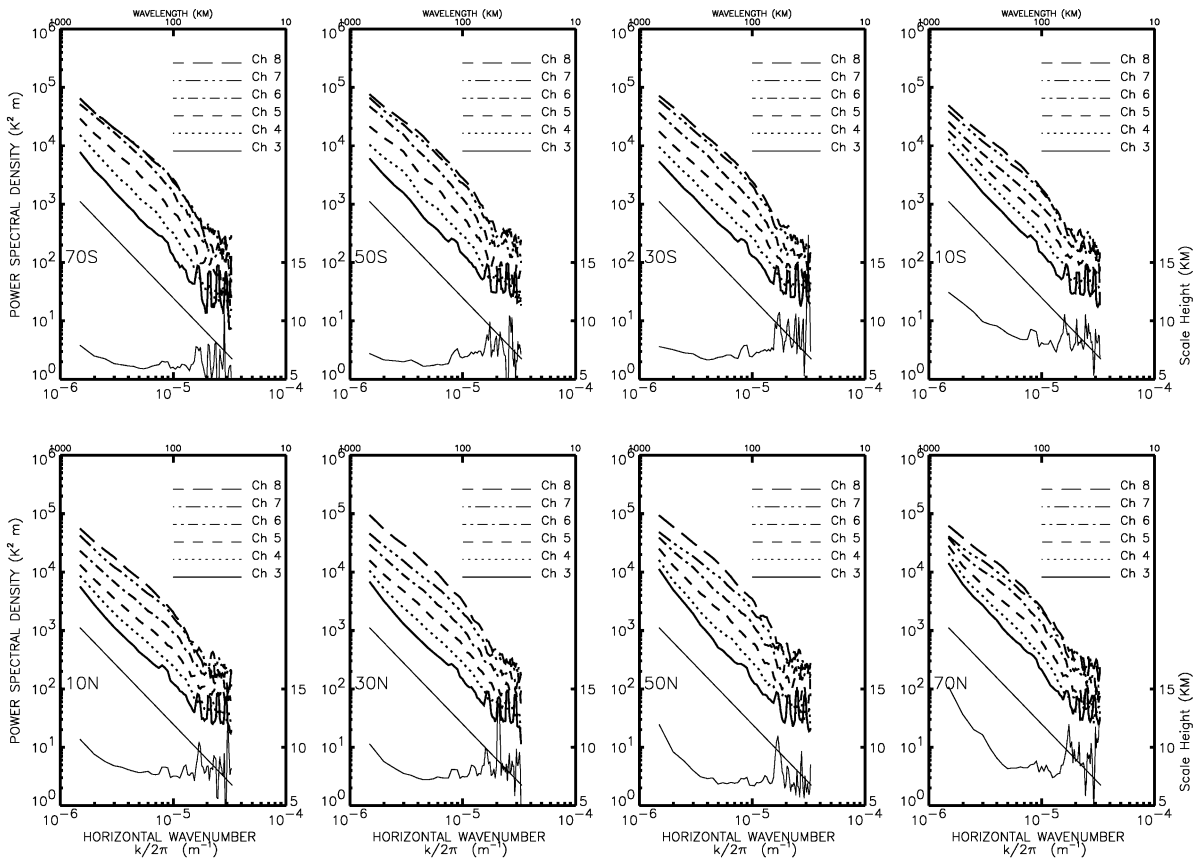
Fig. 4. (*continued*)

4.1. MLS radiance observations and limitations

MLS radiance fluctuations are the convolution of atmospheric temperature perturbations and the instrument temperature weighting function. As discussed in WW97, brightness temperature T_b at tangent height h_t can be obtained by integrating atmospheric temperature T over the instrument weighting function W:

$$T_b(h_t) = \int T(x,z) W(x,z,h_t) \, \mathrm{d}x \, \mathrm{d}z. \tag{1}$$

Since the instrument weighting function is relatively broad, the brightness temperature perturbation T_b' does not respond to small-scale atmospheric temperature perturbations T' in a perfect manner. For example, a wave of 1K in amplitude and 15 km in vertical wavelength would be seen as 0.06K in the limb radiances, or $0.0036K^2$ in the 6-point variance (that is the total spectral power of scales less than $\sim 100\,\mathrm{km}$). Thus, MLS efficiency of measuring atmospheric temperature fluctuations is not very good and reduces sharply with decreasing vertical wavelength. Despite this poor ef-

ficiency factor, a weak variance (e.g., due to waves of 1K and 15 km vertical wavelength) may still be detectable with good instrument noise figure. An analysis by WW97 showed that a $10^{-3}K^2$ variance is measurable with MLS channel 2 after a monthly average, and $\sim 2 \times 10^{-2}K^2$ with channel 6. For the aforementioned reasons, this efficiency factor must be taken into account when interpreting MLS variances.

Another limitation is the UARS MLS sampling bias that could produce variances or power spectra with waves only propagating in certain directions. In the situation of a strong background wind or highly guided wave propagation, such bias could give rise to large differences in the spectral amplitude that depend upon observing geometry. To minimize such bias, the spectra from ascending and descending orbits are averaged together in this analysis. Therefore, the net bias due to viewing geometry is thought to be small compared to latitudinal and seasonal variations.

Missing data may have artifacts on the radiance spectra analyzed. With this concern we simulated effects of

missing data on the derived radiance spectra using artificial data on the same sampling grid. For MLS limb-tracking observations, three missing data points are reported in every 16 measurements due to instrument calibration and antenna adjustment. Since the data gaps are filled with linear interpolations, spectral power leakage may occur. We have identified the following effects with the interpolation of such missing data. First, the simulations suggest that the missing data would produce slightly lower amplitudes at wavelengths near 60 km, similar to what has been seen in Figs. 3 and 4. Second, the interpolation of missing data will cause spectral power leakage. The white noise will be inflated at the end of long wavelengths by a factor of 2. Since the white noise is relatively unimportant for large-scale wave components, the inflation does not affect the spectral power and slope significantly. Third, the spectral power leakage from large scales to small scales is important and the pre-whittening method produces a better result in terms of minimizing the leakage. As a result of spectral power leakage, spectral slope would be slightly steeper and spectral power would be somewhat higher if the pre-whittening treatment were not applied.

Error sources of the radiance fluctuations need to be known accurately so that the weak atmospheric contribution can be derived with good confidence. This is not always achievable since the instrument noise and other unknown radiance errors can become much greater than the atmospheric signals. In addition to the instrument noise, the percentage of unsaturated radiances is another important error source that degrades the spectra analyzed. This error arises as MLS pointing moves off ~2 km above 18 km tangent height in seconds. Channels 1–2 (or 14–15) are most sensitive to such error because of lower saturation altitudes and weaker wave amplitudes. Even for the saturated radiances, rapid pointing movement would cause additional radiance changes because of slightly different temperature weighting functions. However, such a situation does not happen frequently during the limb-tracking observation and hence is negligible for largely averaged spectra.

4.2. Horizontal wavenumber spectrum

One of the key questions about MLS radiance variances and power spectra is what causes the near-zero growth of MLS radiance fluctuations in upper stratosphere and mesosphere? This has been discussed extensively in the recent studies (for a clear vertical profile, the reader is referred to Fig. 4 in WW96b and Fig. 4b in Alexander (1998)). WW96b thought that the near-zero growth of MLS radiance variance is caused primarily by gravity wave saturation/breaking while the interpretation in Alexander (1998) emphasizes Doppler-shifting effects of the background winds on the vertical wavenumber spectrum. Although the reality may involve both processes, the two mechanisms differ fundamentally in terms the cause-and-effect relation between the radi-

ance variance change and the background wind change with height. The interpretation with wave saturation suggests that the near-zero variance growth is a consequence of wave breaking. Therefore, the gravity waves detected by MLS are subject to critical-level filtering in the lower mesosphere, and would be responsible for the slowdown and closure of the stratospheric jet at those altitudes. On the other hand, the interpretation with the Doppler-shifting theory thinks that the near-zero growth is an effect of the background wind change, which is due to a shift of the vertical wavenumber spectrum into or out of MLS filter. More detailed and quantitative description on such mechanism can be found in Alexander (1998). According to the Doppler-shifting interpretation, it is not necessary to have wave saturation/breaking at these altitudes, nor to relate a slowdown/closure of the jet-stream in the mesosphere to the zero growth of the radiance variance.

We should point out here that the wave saturation/breaking interpretation proposed by WW96b and WW97 is consistent with expectations of gravity wave propagation and saturation theory. This interpretation assumes that the gravity waves observed by MLS are dominated by those having horizontal phase velocities opposite to the stratospheric jet-streams. Because of the presence of the background winds, waves with other propagating directions are strongly filtered out. The stratospheric winds provide a favorable condition over 2–3 scale heights for the selected waves to propagate upwards near freely. Such free propagation is reflected in the exponential growth of the wave amplitudes seen in MLS spectral power or variance in the upper stratosphere. It is then speculated that the near-zero growth at 48–60 km in the high-latitude winter could be a manifestation of saturation/breaking of these fast-growing gravity waves as their amplitudes become very large and unstable. One may estimate the normalized radiance variance $(T_{b}'/T_{b})^2$ corresponding to saturated wave amplitudes in the mesosphere based upon a simple linear theory. Let us assume that nearly saturated waves satisfy

$$\frac{T'}{T} = -\frac{ik}{m\omega}\frac{N^2}{g}u' \tag{2}$$

or considering $k = m\omega/N$,

$$\frac{T'}{T} = -i\frac{N}{g}u', \tag{3}$$

where m is the vertical wavenumber, N is the Brunt–Väisälä frequency, k is the horizontal wavenumber, ω is the phase speed, and u' is the perturbation of horizontal velocity. In the case of convective instability, one may assume under wave breaking conditions

$$u' \sim |c - \bar{u}| = N/m, \tag{4}$$

which yields

$$\left(\frac{T'}{T}\right)^2 \sim \left(\frac{N^2}{gm}\right)^2, \tag{5}$$

where c is the phase velocity of gravity wave relative to the ground and $\bar{u}$ is the background wind velocity. For $\lambda_z = 15$ km, from Eqs. (1) and (5), we obtain $(T_b'/T_b)^2 \sim 0.0036(T'/T)^2 \sim 10^{-5}$, which is close to the measured saturation ratio (2–4×10^{-6}) of the 6-point variance (WW96b). Given other uncertainties associated with gravity wave spectra, therefore, it is reasonable to expect significant wave saturation/breaking at 50–60 km altitudes.

On the other hand, modulation by the background wind is an important process for interpreting the stratospheric radiance variances observed by MLS (WW96b). The Doppler-shifting described by Alexander (1998) serves as an effective mechanism that can produce the magnitude of the variance and spectral modulations seen by MLS. Alexander (1998) showed with model simulations that shifting the vertical wavenumber spectrum into and out of MLS filter with the background winds can produce a latitudinal distribution similar to what is observed in MLS variances. It seems clear that the Doppler-shifting of the vertical wavenumber spectrum is the major cause of the radiance variance variations in the stratosphere. Using the concept of the Doppler-shifted vertical wavenumber spectrum, one can successfully explain many features of seasonal and latitudinal variations of the radiance spectra observed in the stratosphere. For example, the large growth rate at 50–70°N during DJF could be attributed to the combined effort of free propagation and the Doppler-shifting. Another example is the DJF spectra at 10–50°S where the scale heights are 7.5 km or less in the upper stratosphere. This growth rate is not surprising if one considers that the radiance fluctuations at these latitudes are dominated by eastward-propagating gravity waves, where nearly free propagation is expected under the westward wind condition. However, in the lower mesosphere, Doppler-shifting is competing with other wave saturation/breaking processes, and the latter plays an increasingly important role at higher levels. In the middle and upper mesosphere, wave saturation and breaking are likely the dominant processes in controlling the radiance and spectra observed by MLS. It requires further quantitative studies to determine to what extent the near-zero growth at 50–60 km is due to the Doppler-shifting of the vertical wavenumber spectrum and how much is contributed by wave breaking/saturation.

Another interesting feature in the MLS horizontal wavenumber spectra is the scale-dependent amplitude growth in the stratosphere that is measured by the scale height in Figs. 3(b) and 4(b). In several cases (mostly in the winter hemisphere) the scale height decreases with increasing wavenumber, yielding poorer efficiency for long-wave propagation in the stratosphere. One interpretation would be the filtering effect of the background winds on waves mixed with eastward and westward propagation. Hamilton (1991) showed in a study of rocket data that gravity waves at mid-latitudes have a very strong tendency for dominant

eastward propagation in summer but a less pronounced westward propagation in winter. Since MLS measures the total spectral power that consists of both eastward and westward propagation, the growth of the spectrum with height depends upon different filtering effects and combinations with these waves. In winter, westward propagation is favored by the prevailing eastward winds in the stratosphere but eastward propagating waves, which might contribute a large part of the MLS spectra, are subject to the filtering by the background winds. Hence, a larger-scale height is generally observed in winter because the filtering on eastward propagating components. One may expect more eastward propagating waves in the lower stratosphere than at upper levels. Also, as noted in channel 3 spectra, the spectral slope is steeper in winter than in summer, which could mean that winter eastward propagation contain more large-scale waves than small ones, leading to more reduction in the spectral growth at long wavelengths. This is a simple interpretation, and other explanations may exist for the scale-dependent growth of MLS horizontal-wavenumber power spectra. For example, the eastward propagating planetary waves seen in the lower stratosphere and troposphere (e.g. Randel, 1987) may have influence on the MLS spectra and the growth rates of the spectral power density.

Meridionally propagating waves can also cause strong disturbances at high latitudes as seen in Fig. 2(a), which received little attention in early gravity wave studies. These waves may be reflected or absorbed at a latitude where there exists a strong jetstream. Sato et al. (1999) analyzed the spectra from a high-resolution general circulation model (GCM) simulation and found that a significant portion of wave activity at high latitudes came from poleward wave propagation in the mid-latitude lower stratosphere. Consider that gravity waves obey the approximate dispersion relation near a jet flow $\bar{u}$ (Fritts, 1984):

$$m^2 = N^2/(c - \bar{u})^2 - k^2. \qquad (6)$$

A strong jetstream could change sign of the left-hand side of Eq. (6) from positive to negative such that the gravity wave is reflected or absorbed. MLS has a good chance to observe such reflection/absorption because the vertical wavelength of these waves would be very large (or small m) at/near the reflection latitude. The example in Fig. 2(a) may likely be one of such wave reflection/absorption cases near a strong jetstream. In addition, MLS often observed greater wave amplitudes when the background wind was large. In Fig. 2(b), the wave appears to have a horizontal wavelength of ~ 1200 km and phase tilted poleward with respect to height. This horizontal wavelength seems consistent with the expectation of the GCM study (Sato et al., 1999), which suggests that the period of these waves should be ~ 20 h and latitude-dependent.

Most of MLS horizontal spectra hold a slope of -2 in the regions where planetary wave activity is weak. The slope of -2 is also reported in aircraft measurements in spite of

very different techniques and vertical resolutions. However, explanations of the MLS spectral slope may be complicated by the processes involving MLS sampling, weighting function filtering, and gravity wave propagation/saturation. For instance, one must take into account the coupling between horizontal and vertical wavenumber spectra because of the shape of MLS weighting functions. Since MLS weighting functions cut off at vertical wavelengths of ~ 10 km, it is not clear to what extent that the observed horizontal wavenumber spectra are correlated with vertical wavenumber spectra. Also, it is not clear what mechanisms are controlling the horizontal spectra although several theories have been proposed, including interpretations based upon two-dimensional turbulence (e.g. Lilly, 1983; Gage and Nastrom, 1985), diffusive filtering theory (Gardner, 1994) and saturated cascade theory (Dewan, 1997).

5. Summary

We have presented the horizontal wavenumber spectra of MLS limb-tracking radiances at scales between 30 and 800 km and compiled a seasonal climatology of the spectra for 6 altitudes and 8 latitudes during DJF and MAM seasons. Major features revealed by these analyses are:

(1) MLS saturated radiances from the limb-tracking observation captured many wave-like temperature oscillations that show clearly organized phase lines both tilted and fixed with respect to height. The radiance fluctuations are sometimes correlated at different altitudes and show a significant amplitude growth with height between 38 and 51 km.

(2) Most of the horizontal wavenumber spectra have a slope of around -2, while some vary between below -2 in a quiet atmosphere or steeper than -3 in wave-active regions. The amplitude of the spectra generally grows rapidly with height between 38 and 61 km but exhibit less or near-zero growth above that altitude.

(3) The amplitude growth is scale-dependent in the stratosphere showing less efficient propagation for large-scale waves. The most efficient propagation is found with small-scale waves in the SH during DJF, showing a scale height of 6–7 km, which suggests the free propagation of such waves in the middle atmosphere.

We also attempted to interpret some characteristics of the MLS radiance variances and the power spectra of horizontal wavenumber, most importantly, the zero growth of these variables in the mesosphere. We think that the phenomenon is a manifestation of saturation/breaking of the gravity waves that propagate through the stratosphere having phase velocities opposite to the background winds. On the other hand, the Doppler-shifting on vertical wavenumber spectra is an important mechanism for modulating the radiance variance and power spectra seen in the stratosphere.

References

Alexander, M.J., 1998. Interpretations of observed climatological patterns in stratospheric gravity wave variance. Journal of Geophysical Research 103, 8627–8640.

Allen, S.J., Vincent, R.A., 1995. Gravity wave activity in the lower atmosphere: seasonal and latitudinal variations. Journal of Geophysical Research 100, 1327–1350.

Bacmeister, J.T., et al., 1996. Stratospheric horizontal wavenumber spectra of winds, potential temperature, and atmospheric tracers observed by high-altitude aircraft. Journal of Geophysical Research 101, 9441–9470.

Balsley, B.B., Carter, D.A., 1982. The spectrum of atmospheric velocity fluctuations at 8 km and 86 km. Geophysics Research Letters 9, 465–468.

Blackman, R.B., Tukey, J.W., 1958. The Measurement of Power Spectra. Dover, New York, p. 190.

Dewan, E.M., 1997. Saturated-cascade similitude theory of gravity wave spectra. Journal of Geophysical Research 102, 29,799–29,817.

Dewan, E.M., Good, R.E., 1986. Saturation and the "universal" spectrum for vertical profiles of horizontal scalar winds in the atmosphere. Journal of Geophysical Research 91, 2742–2748.

Eckermann, S.D., Hirota, I., Hocking, W.K., 1994. Gravity wave and equatorial wave morphology of the stratosphere derived from long-term rocket soundings. Quarterly Journal of Royal Meteorological Society 121, 149–186.

Fetzer, E.J., Gille, J.C., 1994. Gravity wave variance in LIMS temperatures. Part I: variability and comparison with background winds. Journal of Atmospheric Science 51, 2461–2483.

Fritts, D.C., 1984. Gravity wave saturation in the middle atmosphere: A review of theory and observations. Review of Geophysics 22, 275–308.

Fritts, D.C., Blanchard, R.C., Coy, L., 1989. Gravity wave structure between 60 and 90 km inferred from shuttle reentry data. Journal of Atmospheric Science 46, 423–434.

Fukao, S., et al., 1994. Seasonal variability of vertical eddy diffusivity in the middle atmosphere, 1. three-year observations by the middle and upper atmosphere radar. Journal of Geophysical Research 99, 18,973–18,987.

Gage, K.S., 1979. Evidence for a k-5/3 power law inertial range in mesoscale two-dimensional turbulence. Journal of Atmospheric Science 36, 1950–1954.

Gage, K.S., Nastrom, G.D., 1985. On the spectrum of atmospheric velocity fluctuations seen by MST/ST radar and their interpretation. Radio Science 20, 1339–1347.

Gardner, C.S., 1994. Diffusive filtering theory of gravity wave spectra in the atmosphere. Journal of Geophysical Research 99, 20,601–20,622.

Hamilton, K., 1991. Climatological statistics of stratospheric inertia-gravity waves deduced from historical rocketsonde wind and temperature data. Journal of Geophysical Research 96, 20,831–20,839.

Hines, C.O., 1991. The saturation of gravity waves in the middle atmosphere. II: development of Doppler-spread theory. Journal of Atmospheric Science 48, 1360–1379.

Hirota, I., 1984. Climatology of gravity waves in the middle atmosphere. In: Holton, J.R., Matsuno, T. (Eds.), Dynamics of the Middle Atmosphere. Terra, Tokyo, pp. 65.

Holton, J.R., 1982. The role of gravity wave induced drag and diffusion in the momentum budget of the mesosphere. Journal of Atmospheric Science 39, 791–799.

Lilly, D.K., 1983. Stratified turbulence and the mesoscale variability of the atmosphere. Journal of Atmospheric Science 40, 749–761.

Lindzen, R.S., 1981. Turbulence and stress owing to gravity wave and tidal breakdown. Journal of Geophysical Research 86, 9707–9714.

Manson, A.H., Meek, C.E., 1986. Dynamics of the middle atmosphere at Saskatoon (52°N, 107°W): a spectral study during 1981,1982. Journal of Atmospheric and Solar-Terrestrial Physics 48, 1039–1055.

Matsuno, T., 1982. A quasi-one-dimensional model of the middle atmospheric circulation interacting with internal gravity waves. Journal of Meteorological Society of Japan 60, 215.

Nastrom, G.D., Gage, K.S., 1985. A climatology of atmospheric wave number spectra observed by commercial aircraft. Journal of Atmospheric Science 42, 950–960.

Randel, W.J., 1987. A study of planetary waves in the southern winter troposphere and stratosphere. Part I: Wave structure and vertical propagation. Journal of Atmospheric Science 44, 917–935.

Sato, K., Kumakura, T., Takahashi, M., 1999. Gravity waves appearing in a high-resolution GCM simulation. Journal of Atmospheric Science 56, 1005–1018.

Smith, S.A., Fritts, D.C., VanZandt, T.E., 1987. Evidence for a saturated spectrum of atmospheric gravity waves. Journal of Atmospheric Science 44, 1404–1410.

Swenson, G.R., et al., 1995. ALOHA-93 measurements of intrinsic AGW characteristics using airborne airglow imager and groundbased Na Wind/Temperature Lidar. Geophysics Research Letters 22, 2841–2844.

VanZandt, T.E., 1982. A universal spectrum of buoyancy waves in the atmosphere. Geophysics Research Letters 9, 575–578.

Vincent, R.A., Fritts, D.C., 1987. A climatology of gravity wave motions in the mesopause region at Adelaide, Australia. Journal of Atmospheric Science 44, 748–760.

Weinstock, J., 1990. Saturated and unsaturated spectra of gravity waves and scale dependent diffusion. Journal of Atmospheric Science 47, 2211–2225.

Wilson, R., Chanin, M.L., Hauchecorne, A., 1991. Gravity waves in the middle atmosphere observed by Rayleigh Lidar: 2. Climatology. Journal of Geophysical Research 96, 5169–5183.

Wu, D.L., Waters, J.W., 1996a. Satellite observations of atmospheric variances: A possible indication of gravity waves. Geophysics Research Letters 23, 3631–3634.

Wu, D.L., Waters, J.W., 1996b. Gravity-wave-scale temperature fluctuations seen by the UARS MLS. Geophysics Research Letters 23, 3289–3292.

Wu, D.L., Waters, J.W., 1997. Observations of gravity waves with the UARS microwave limb sounder. In: Hamilton, K. (Ed.), Gravity Wave Processes and Their Parameterization in Global Climate Models, NATO ASI Series, Vol. 50. Springer, New York, pp. 404.

Wu, Y.-F., Widdel, H.-U., 1991. Further study of a saturated gravity wave spectrum in the mesosphere. Journal of Geophysical Research 96, 9263–9272.